Pressure-induced ferroelastic instability and lattice dynamics of Cs_2HgCl_4 crystals within the semiempirical rigid-ion model

A. V. Kityk, Ya. I. Shchur, A. V. Zadorozhna, I. B. Trach, I. S. Girnyk, I. Yu. Martynyuk-Lototska, and O. G. Vlokh
Institute of Physical Optics, Dragomanova str 23, 290005 Lviv, Ukraine
(Received 23 December 1997)

An analysis of the lattice dynamics of Cs_2HgCl_4 crystals and their relation to the pressure-induced proper ferroelastic instability is reported using a semiempirical rigid-ion model in the quasiharmonic approximation. The model parameters (effective radii and charges of ions) have been adjusted to satisfy the equilibrium configuration of the observed structure in the normal phase. The influence of unharmonicity has been introduced into the lattice dynamics simulation indirectly through the changes of the lattice parameters that occur under the action of temperature and hydrostatic pressure. Such a simple model reproduces the lattice instability leading to the appearance of the proper ferroelastic phase. It has been shown that the lattice loses its stability with respect to the transverse-acoustical mode $TA_Z(\mathbf{k}\|\mathbf{b})$ whereas the soft optical mode (B_{3g} symmetry at $\mathbf{k}=0$) remains stable. This is in agreement with the phenomenological theory. The rigid-ion model also reproduces the line of the proper ferroelastic phase transitions in the P,T-phase diagram which is close to the experimentally observed phase diagram. [S0163-1829(98)03729-1]

I. INTRODUCTION

At atmospheric pressure the Cs_2HgCl_4 crystal possesses a series of structural phase transitions including two transitions into the incommensurate phase. The initial (normal) phase of Cs_2HgCl_4 has α-K_2SO_4-type structure with a space group of symmetry D_{2h}^{16} ($Pnma$) and four formula units per unit cell.[1] On cooling this crystal undergoes six successive phase transitions at $T_I=220$ K, $T_C=195$ K, $T_1=184$ K, $T_2=182$ K, $T_3=166$ K, and $T_4=164$ K.[2] According to the results of nuclear magnetic resonance measurements[3] the system exhibits the incommensurate phase between T_I and T_C. Acoustic and optical measurements were used in the investigation of the pressure-temperature (P-T) phase diagram of Cs_2HgCl_4 crystals.[4] It was shown that the incommensurate phase in the P-T phase diagram ends in the triple point at $P_K\approx 140$ MPa and $T_K\approx 220$ K, where the two lines of the incommensurate phase transitions merge into one line of the ferroelastic phase transitions. The anomalous decrease in the velocity of the pure transverse-acoustic wave V_4 (relevant elastic constant $C_{44}=\rho V_4^2$) which occurs at $P>P_K$ in the vicinity of the direct phase transition from the normal into the ferroelastic phase[4] (Fig. 1) clearly indicates that this pressure-induced phase is proper ferroelastic phase with the component of the spontaneous deformation $U_{YZ}=U_4$. Thus inhomogeneous (incommensurate) structural ordering changes at $P>P_K$ into the homogeneous ferroelastic ordering. The nature of the corresponding triple point in the P-T phase diagram of Cs_2HgCl_4 crystals has been considered in detail only within the framework of the phenomenological theory,[4,5] whereas the microscopical aspects of this phenomena remain unknown.

It is necessary to remember that the proper ferroelastic phase with a component of spontaneous deformation U_4 in Cs_2HgCl_4 crystals appears at relatively low hydrostatic pressure (above 10 MPa).[4] However, only at the triple point (P_K,T_K), does the line of the first-order phase transitions from the incommensurate to proper ferroelastic phase (space group $P2_1/a11$) in the P-T phase diagram change into the line of the second-order phase transition from the normal phase into the proper ferroelastic phase. Therefore, at $P>P_K$ the ferroelastic instability can be considered within the semiempirical rigid-ion model using the well-known soft-mode concept.[6] This concept is based on the principle of lattice stability according to which the lattice remains stable if all the frequencies of the normal phonon modes $\omega_i(\mathbf{k})$ are real for any wave vector $\mathbf{k}$ in the Brillouin zone. The lattice loses its stability when the frequency of some phonon mode (soft mode) tends to zero at a certain value of temperature and pressure. Accordingly, the second-order structural phase transition is usually considered as a condensation of the soft optical mode. However, in the case of proper ferroelastic phase transitions some peculiarities of lattice instability can be expected because of the bilinear coupling between the soft optical normal coordinate and deformation. This causes the critical slowing down of the transverse acoustic phonons in

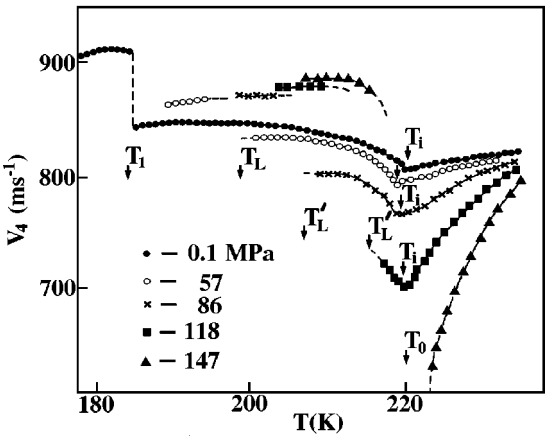

FIG. 1. The temperature dependence of shear ultrasonic velocity $V_4(\mathbf{k}\|[010], \mathbf{e}\|[001])$ of Cs_2HgCl_4 crystals at different pressures P (Ref. 4).

the region of the phase transition from the normal to the ferroelastic phase (Fig. 1). Thus, the lattice loses its stability with respect to the acoustical vibration whereas the frequency of the soft optical mode remains positive and real at the phase-transition point T_0. Although this fact is known in the phenomenological theory, it has never been considered from a microscopic point of view. Clear understanding of the microscopic mechanism of the pressure-induced ferroelastic instability in Cs_2HgCl_4 crystals is also very important from the viewpoint of a nature of the triple point in the P-T phase diagram in which the incommensurate instability changes into the proper ferroelastic one.

In this paper we present the theoretical treatment of the lattice dynamics of Cs_2HgCl_4 crystal within the framework of the rigid-ion model in the harmonic approximation for the normal phase. Our attention is devoted to the ferroelastic instability which occurs under applied hydrostatic pressure. We have restricted the analysis to the low-frequency external phonon modes which give the most complete information about the nature of the pressure-induced proper ferroelastic phase transition. The phonon spectra calculations were performed at different values of hydrostatic pressure and temperatures. Influence of the interatomic unharmonicity was introduced indirectly through the changes of the lattice parameters a,b, and c, which have been determined in each case from the experimental data of ultrasonic and dilatometric (presented below) measurements. The results of the microscopical consideration are compared with the sequences of phenomenological theory and experimental data.

II. *P*-*T* PHASE DIAGRAM

The $P-T$ phase diagram of Cs_2HgCl_4 crystals was determined by Kityk *et al.*[4] for the pressure region of $0.1-180$ MPa using the acoustical method. In the present work we have expanded the range of applied pressures up to 570 MPa. The acoustical measurements have been performed on a single Cs_2HgCl_4 crystals which were grown from melt by the Bridgman method. We used the following crystallographic orientation: $c>a>b$ ($c\approx\sqrt{3}b$, where a is the pseudohexagonal axis). The size of the plane parallel specimens was typically of $4\times4\times4$ mm^3. Relative velocity changes of the longitudinal ultrasonic waves were measured by the pulse-echo overlap method[7] with an accuracy of the order of $10^{-4}-10^{-5}$. The accuracy of the absolute velocity determination was about 0.5%. The acoustic waves in the samples were excited by $LiNbO_3$ transducers with the resonance frequency $f=10$ MHz, bandwidth $f=0.1$ MHz, and acoustic power $P_A=1-2W$. The acoustic investigations have been performed at constant values of hydrostatic pressure with the rate of temperature change of about 0.3 K/min.

Figure 2 shows the isobaric temperature dependences of the longitudinal ultrasonic wave velocity $V_3(\mathbf{k}\|[001], \mathbf{e}\|[001])$ at different pressures P. The phase transitions from the normal to the proper ferroelastic phase are clearly manifested in the anomalous changes in $V_3(T)$ near T_0. The temperature of the ferroelastic phase transition increases under the applied hydrostatic pressure. In the high-pressure region, the phase transition from the proper ferroelastic phase to phase V (in the notation of Ref. 4) is observed at $T=T_5$. The

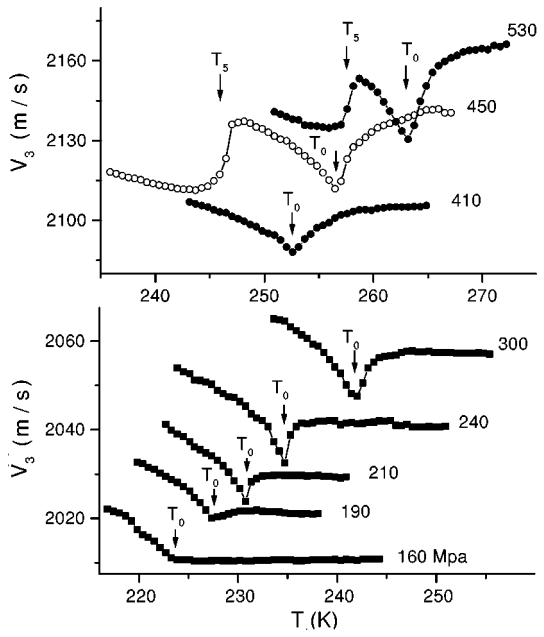

FIG. 2. The temperature dependence of the longitudinal ultrasonic wave velocity $V_3(\mathbf{k}\|[001], \mathbf{e}\|[001])$ of Cs_2HgCl_4 crystals at different pressures P.

origin of phase V is still unknown. Using the results of our previous measurements[4] and data shown in Figs. 1 and 2, one can present the P-T phase diagram in the form shown in Fig. 3 for the hydrostatic pressures $0.1-570$ MPa. As the pressure increases, the temperature region of proper ferroelastic phase becomes narrower. At the hydrostatic pressure about 600 MPa, one can expect in Cs_2HgCl_4 crystals another polycritical point where the proper ferroelastic phase would disappear. This polycritical point has not been observed in our experiment since the crystal samples are cracked at $P>570-580$ MPa.

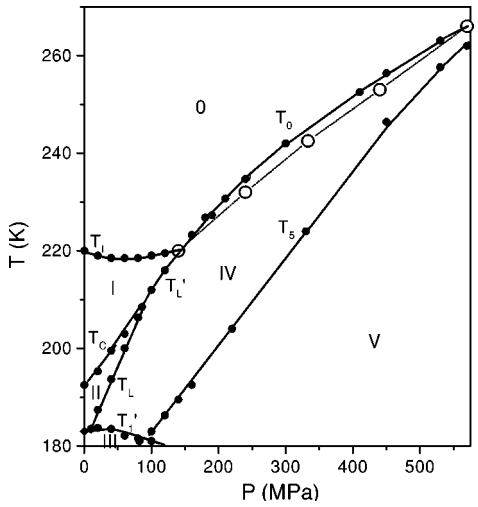

FIG. 3. $P-T$ phase diagram of Cs_2HgCl_4 crystals: 0 is the normal phase, I is the incommensurate phase, II is the improper ferroelectric phase, III is the improper ferroelastic phase, IV is the proper ferroelastic phase, V is the unknown monoclinic phase; $\cdot\cdot\bigcirc\cdots\bigcirc\cdot\cdot$ $T_0(P)$ is the line calculated within the rigid-ion model.

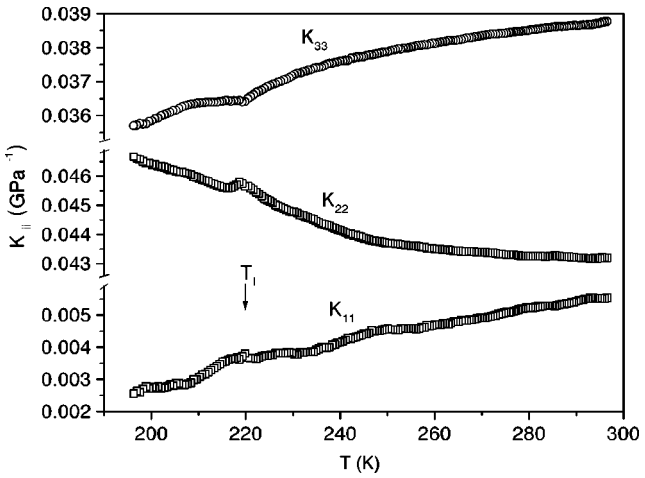

FIG. 4. The temperature dependences of the linear compressibility constants K_{ii} of Cs_2HgCl_4 crystals.

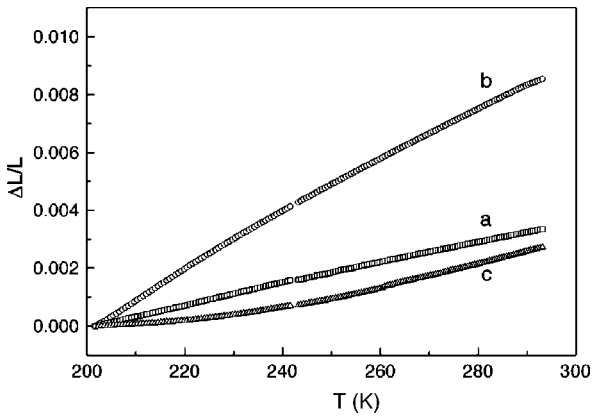

FIG. 5. Thermal expansion of Cs_2HgCl_4 crystals along the principal crystallographic axis.

III. THERMAL EXPANSION AND LATTICE COMPRESSIBILITY

The microscopic and semimicroscopic considerations of the lattice instability induced by high hydrostatic pressure are frequently based on the computer simulation of the lattice dynamics within the rigid-ion model in the harmonic approximation. The influence of the unharmonicity, which causes the lattice instability at the structural phase transition, can be introduced into this simulation indirectly through the changes of the lattice parameters under hydrostatic pressure and temperature. The coefficients of the lattice compressibility and thermal expansion, which are necessary in this case, have been determined from the acoustical and dilatometric measurements. Our previous ultrasonic investigations[4,8] were recently completed by measurements for several additional geometries of ultrasonic propagation in order to obtain complete elastic constant tensor C_{ij}.[9] Using this tensor we have determined the tensor coefficients of the linear compressibility K_{ij}. One can note that the tensor of compressibility constants in the normal and incommensurate phases contains only diagonal components K_{11}, K_{22}, and K_{33}, whereas $K_{ij}=0$ for $j\neq i$. The temperature dependences of the compressibility constants $K_{ii}(T)$ obtained in such a way are presented in Fig. 4. One can see that the anomalies near T_I are more or less clearly observed in the temperature dependences of $K_{22}(T)$ and $K_{33}(T)$. Contrary to expectations, the anomalous changes of the compressibility constants K_{ii} are continuous in the region of T_I. This unusual behavior is attributed to the fluctuation effects. The detailed phenomenological consideration is given in Ref. 9.

The thermal expansion of Cs_2HgCl_4 crystals along the principal crystallographic axes was measured using capacitance dilatometer. The plane-parallel specimens are typically $8\times8\times8$ mm^3 in size. The accuracy of the dilatometric measurements was about 2 nm. Figure 5 shows linear thermal expansion ($\Delta L/L$) as a function of temperature. As one can see from this figure, $\Delta L/L$ along the b axis is essentially larger than $\Delta L/L$ measured along the a or c direction. The kinks of the temperature dependences $\Delta L/L$ that usually would be expected in the region of phase transition from the normal to the incommensurate phase, are not observed. We assume that such a behavior is caused by the strong influence of fluctuation effects as well as small values of coupling constants a_i corresponding to the interaction between the deformation components U_i and order parameter Q (U_iQ^2-type coupling). In this respect, the dilatometric measurements are in a good agreement with the ultrasonic data.[9]

IV. PHONON SPECTRA OF Cs_2HgCl_4 CRYSTALS ($T=293$ K, $P=0.1$ MPa)

In this paper our attention will be devoted to the ferroelastic instability which occurs under the applied hydrostatic pressure. Only the external vibration would play a main role in the lattice-dynamical model of the ferroelastic instability. Thus, we performed the lattice dynamics simulations using the simple rigid-ion model with the $HgCl_4^{2-}$ groups reduced to rigid bodies. This model implies consideration of the translational vibration of Cs^+ ions as well as translational and rotational vibrations of the tetrahedral groups $HgCl_4^{2-}$. The internal degrees of freedom connected with deformation of the tetrahedral groups are neglected. The unit cell in the normal phase contains eight Cs^+ ions and four $HgCl_4^{2-}$ tetrahedral groups.[1] There are therefore 48 external modes, which can be classified in the Brillouin-zone center as 36 translational modes ($6A_g+3B_{1g}+6B_{2g}+3B_{3g}+3A_u+6B_{1u}+3B_{2u}+6B_{3u}$) and 12 rotational modes ($A_g+2B_{1g}+B_{2g}+2B_{3g}+2A_u+B_{1u}+2B_{2u}+B_{3u}$). The compatibility relations between the irreducible representation along the symmetrical Δ direction ($\mathbf{k}=\mu\mathbf{b}^*$, $0<\mu<1/2$) are presented in Table I. This direction is especially important in our considerations because it contains the transverse-acoustic mode TA_Z. The symmetry of this mode at the Δ line is the same as the symmetry of the soft optical mode, which is the essential reason for the ferroelastic instability, as will be shown below.

Numerical modeling of the lattice dynamics of Cs_2HgCl_4 crystals has been performed using the modified program DISPR.[10] The potential energy Φ of the interatomic interactions has been considered as a sum of two contributions:

TABLE I. Compatibility relation between the irreducible representations along the *b* axis for the *Pnma*, space group.

$\mathbf{k}=0$	$\mathbf{k}=\mu\mathbf{b}^*$	$\mathbf{k}=(1/2)\mathbf{b}^*$
$7A_g$	$12\Delta_1$	$24Y_1$
$5B_{2u}$		
$5B_{1g}$	$12\Delta_4$	
$7B_{3u}$		
$7B_{2g}$	$12\Delta_2$	$24Y_2$
$5A_u$		
$5B_{3g}$	$12\Delta_3$	
$7B_{1u}$		

long-range Coulomb and short-range Born-Mayer-type interactions:

$$\Phi=\frac{1}{2}\sum_{\substack{l,k\\k,K}}\sum_{\substack{l',k'\\k',K'}}\frac{1}{4\pi\epsilon_0}\frac{Z(Kk)Z(K'k')e^2}{r(lKk,l'K'k')}+a\,\exp\left\{-\frac{br(lKk,l'K'k')}{R(Kk)+R(K'k')}\right\}, \tag{1}$$

where $a=1822$ eV, $b=12.364$; l, l' are the index numbers of the unit cell; K, K' are the indices of the ion group, k denotes ionic species in the corresponding molecular group; e is the electron charge; r is the distance between the ions with indices K, k and K',k'. The model parameters for the interatomic forces [effective charges $Z(K,k)$ and effective radii $R(K,k)$] which were used in the dynamical analysis, were determined by the condition that the resulting atomic equilibrium configuration would be a good approximation to the observed structure, i.e., according to the crystal structure stability. The corresponding equilibrium configuration is determined by

$$\left.\frac{\partial\Phi}{\partial U_\alpha(l,k)}\right|_0=0 \tag{2}$$

where $U_\alpha(lk)$ is the displacement component in the a direction for the ion with the index number k. The optimization procedure has been performed by taking into account the electrical neutrality condition $[\Sigma_{K,k}Z(K,k)=0]$. Finally we have obtained the following values for the effective parameters:

$$Z(\mathrm{Cs})=0.73,\quad Z(\mathrm{Hg})=0.1,\quad Z(\mathrm{Cl})=-0.39;$$

$$R(\mathrm{Cs})=3.22\ \text{Å},\quad R(\mathrm{Hg})=0.8\ \text{Å},\quad R(Cl)=1.53\ \text{Å}.$$

Figure 6 shows calculated phonon-dispersion curves of Cs_2HgCl_4 crystals within the rigid-ion model at the line Δ ($\mathbf{k}=\mu\mathbf{b}^*$). One can note that the parameters mentioned above satisfy the lattice stability for all external vibrations along the $\Sigma(\mathbf{k}=\mu\mathbf{a}^*)$, $\Delta(\mathbf{k}=\mu\mathbf{b}^*)$, and $\Lambda(\mathbf{k}=\mu\mathbf{c}^*)$ lines. As it can be seen from Fig. 6, the phonon modes are twofold degenerate at the Brillouin-zone boundary, which is in agreement with the compatibility relations shown in Table I. The Raman spectra of the Cs_2HgCl_4 crystals for different scattering geometries at $T=293$ K are shown in Fig. 7. The comparison between the calculated phonon frequencies at the Brillouin-zone center ($\mathbf{k}=0$) and Raman spectroscopy data is presented in Table II. In general, the agreement between the calculations and experiment is within 5–20 %. This can be considered as good agreement if we take into account that the resulting atomic equilibrium configuration has been adjusted using only static structural data.[1]

V. FERROELASTIC INSTABILITY: RIGID-ION MODEL

As it follows from Fig. 6, the phonon spectra of Cs_2HgCl_4 crystals is characterized by the low-frequency optical branch

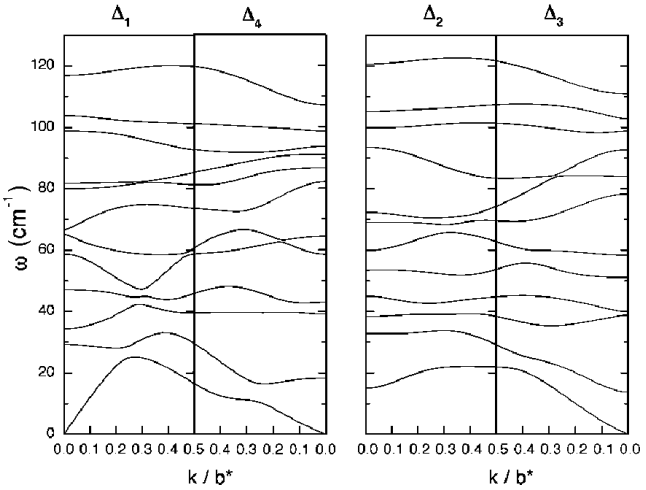

FIG. 6. Phonon spectra of Cs_2HgCl_4 crystals along the symmetrical Δ line ($\mathbf{k}=\mu\mathbf{b}^*$) at $T=293$ K calculated within the rigid-ion model.

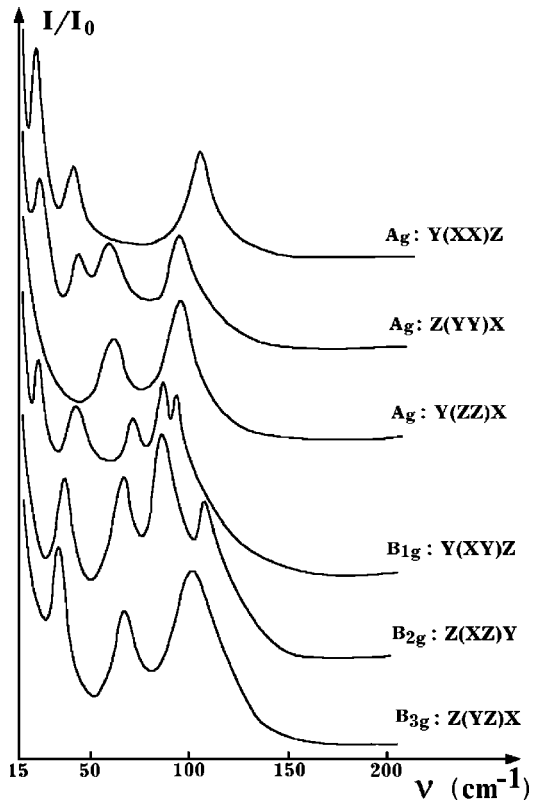

FIG. 7. Low frequency part of Raman spectra of Cs_2HgCl_4 crystals at different scattering geometries.

of B_{3g} symmetry in the center of the Brillouin zone. Following the general symmetry consideration, this mode can be associated with the soft optical mode which is responsible for the proper ferroelastic phase transition. At the same time, we expect that the transverse-acoustical mode TA_Z would play an important role in the ferroelastic instability. Both modes have the same symmetry at the Δ line and therefore, their bilinear coupling is expected to be essential for the ferroelastic phase transition.

Modeling of the ferroelastic instability was carried out through the changes of the lattice parameters a, b, and c, which appear under hydrostatic pressure P and temperature T. The phonon spectra were therefore calculated at different values of temperature and hydrostatic pressure. In each case, we used the harmonic approximation at given values T and P. The lattice parameters for a given value of T and P were determined from the experimental data of the thermal expansion and ultrasonic measurements using the following relations:

$$a=(1-K_{11}P)a_T,$$
$$b=(1-K_{22}P)b_T, \tag{3}$$
$$c=(1-K_{33}P)c_T.$$

Here K_{11}, K_{22} and K_{33} are the linear compressibility constants along the a, b, and c axes, respectively, and a_T, b_T, and c_T are the lattice parameters at temperature T. In our modeling, we used two assumptions concerning the atomic structure distortion. First, we assumed that the temperature and hydrostatic pressure do not influence the fractional atomic coordinates in the unit cell. Second, we considered the tetrahedral $HgCl_4$ groups as undeformed bodies, therefore only the fractional position of Cs and Hg ions have been kept. Lattice-dynamics calculations show, that in the first case we get a gradual rise of all normal mode frequencies as the pressure increases up to 1.2 GPa. Thus any lattice instability, including the ferroelastic one, cannot be obtained in the model with deformed tetrahedral groups.

An opposite situation takes place if we assume that the tetrahedral groups are rigid. In this case, several frequencies of the optical mode, including the lowest one, fall down under the applied hydrostatic pressure. Figure 8 shows a part of the phonon spectra for two fixed temperatures $T=266$ K and 220 K, at different values of the applied hydrostatic pressure P. As the pressure increases, the low-frequency optical mode of B_{3g} symmetry (at $\mathbf{k}=0$) decreases, which is accompanied by decreasing of the slope in the transverse-acoustical branch TA_Z. The slope of the acoustical branch at $\mathbf{k}=0$ equals zero at $P_0=140$ MPa ($T=T_0=220$ K) and $P_0=558$ MPa ($T=T_0=266$ K), which corresponds to the limit of the lattice stability (phase-transition point). The case, with $P=146$ MPa ($T=220$ K), and $P=570$ MPa ($T=266$ K) correspond to the unstable lattice. In order to obtain good agreement between the experimental and calculated values of the phase-transition point (P_0,T_0) in the P-T phase diagram, the effective parameters of the rigid-ion model had to be corrected slightly. From the physical point of view, this procedure is correct if we remember that the effective parameters (charges and radii) are defined by the charge-density distribution, which can be changed with temperature and hydrostatic pressure. In our simulation, we have observed that the effective radius of the Cl-ion essentially influences the lattice stability. We have found that the best agreement between experimental and calculated phase-transition points (T_0, P_0) is obtained with R_{Cl} (140 MPa, 220 K)=1.552 Å and R_{Cl}(558 MPa, 266 K)=1.4 Å, whereas all other parameters remain unchanged. Using these values and assuming a linear dependence of R_{Cl} on pressure and temperature, one obtains

$$R_{Cl}(P,T)=1.552-0.001\,652(T-220)$$
$$-0.000\,181\,8(P-140). \tag{4}$$

Here T is taken in K and P is taken in MPa. Introducing empirical Eq. (4) into the lattice-dynamics calculation we obtain the line of the ferroelastic phase transition $T_0(P)$ in

TABLE II. Raman frequencies of Cs_2HgCl_4: experimental and calculated within the rigid-ion model.

A_g		B_{1g}		B_{2g}		B_{3g}	
Calc.	Expt.	Calc.	Expt.	Calc.	Expt.	Calc.	Expt.
34	24	18	23	38	33	14	
47	43	39	38	54		40	31
59	60	59	67	60	61	58	60
65		91	89	69		78	
82		94	93	93	89	99	94
99	100			100	103		
116	109			120			

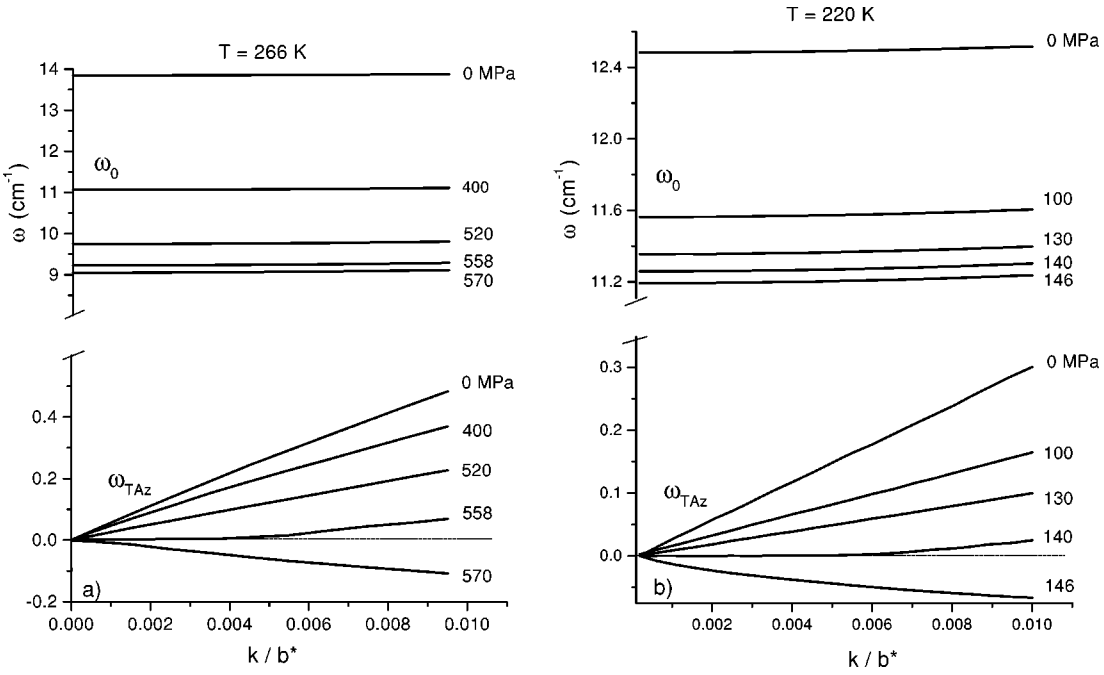

FIG. 8. Part of the calculated phonon spectra of Cs_2HgCl_4 crystals at $T=266$ K (a) and $T=220$ K (b). The soft mode of B_{3g} symmetry (at $\mathbf{k}=0$) and the transverse-acoustic mode TA_Z are shown at different hydrostatic pressures. Curves 0,400,520 MPa (a) and 0,100,130 MPa (b) correspond to the stable lattice; curves 558 MPa (a) and 140 MPa (b) are the points of the ferroelastic instability (the phase-transition point); curves 570 MPa (a) and 146 MPa (b) correspond to the unstable lattice.

the P,T-phase diagram shown by the dashed line in Fig. 3. Agreement between the experiment (solid line) and theory (dashed line) is excellent, taking into account that the pressure-temperature structure distortion has been modeled. Coming back to the evolution of the phonon spectra near the normal-ferroelastic phase transition (Fig. 8), we have to point out a very important peculiarity of these spectra. Taking into account that the slope of the acoustical branch defines the phase velocity of the transverse-acoustical phonons ($V=d\omega_{TA}/d\mathbf{k}$), one can see their critical slowing down at the proper ferroelastic phase transition which is in good agreement with ultrasonic data (see Fig. 1). At the same time, the soft-mode frequency is still real. Therefore, the rigid-ion model clearly confirms the fact that the proper ferroelastic phase transition occurs due to the instability of the acoustical phonons.

VI. FERROELASTIC INSTABILITY: PHENOMENOLOGICAL MODEL

Comparison between the microscopical and phenomenological models is very useful for a better understanding of the mechanism of the ferroelastic phase transition. Obviously, proper ferroelastic instability is caused by the bilinear coupling between the soft optical and acoustical modes, which can be reproduced within the phenomenological theory. To show this, let us consider the quasiharmonic part of the free-energy density:

$$f=\frac{1}{2}A_0(P_C-P)Q^2+\frac{1}{2}\gamma\left(\frac{\partial Q}{\partial y}\right)^2+\alpha Q U_4+\frac{1}{2}C_{44}^0U_4^2. \tag{5}$$

Here, Q is the normal optical phonon coordinate of the B_{3g} symmetry at $\mathbf{k}=0$, $U_4=U_{YZ}$ is the deformation, and C_{44}^0 is the elastic constant far from region of the phase transition ($P\ll P_C$). After inserting $U_4=\partial Z/\partial y$ (Z is the z component of the displacement vector) and taking the Fourier transform, Eq. (5) is

$$F=\int f dy=\sum_k \left\{\frac{1}{2}\omega_0^2(\mathbf{k})Q_kQ_k^*+\frac{1}{2}\omega_{\mathrm{TA}}^2(\mathbf{k})Z_kZ_k^* + i\alpha\mathbf{k}(Z_kQ_k^*-Q_kZ_k^*)\right\}. \tag{6}$$

Here, the normal coordinates Q_k and Z_k correspond to the soft optic and transverse-acoustic modes, respectively; $\omega_0(\mathbf{k})$ and $\omega_{TA}(\mathbf{k})$ are the corresponding ''uncoupled'' mode frequencies that may be presented for small $\mathbf{k}$ as

$$\omega_0^2(\mathbf{k})=A_0(P_C-P)+\gamma\mathbf{k}^2+\cdots, \tag{7}$$

$$\omega_{TA}^2(\mathbf{k})=C_{44}^0\mathbf{k}^2+\cdots. \tag{8}$$

In order to find the dispersion curves of the coupled modes we shall assume that the damping of these modes is small enough and is neglected. One then constructs a Lagrangian using F as the potential energy:

$$L=T-F=\frac{1}{2}\sum_k(\dot{Q}_k\dot{Q}_k^*+\dot{Z}_k\dot{Z}_k^*)-F. \tag{9}$$

The Lagrange equations of motion $(d/dt)(\partial L/\partial\dot{P})-\partial L/\partial P=0$ ($P\equiv Q_k$, Z_k) can be separated into pairs of coupled equations:

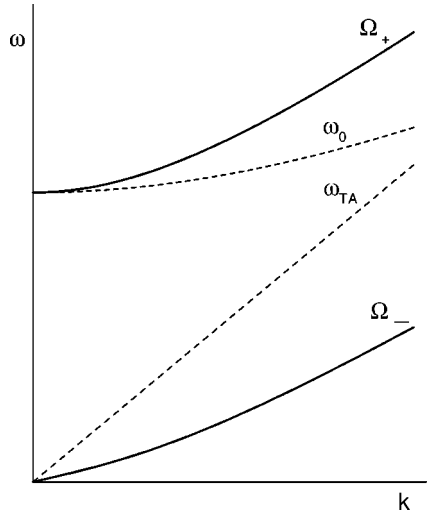

FIG. 9. Schematic representation of dispersion curves resulting from bilinear interaction between the soft optical and transverse-acoustical phonon modes [Eq. (15)]: dashed lines are uncoupled acoustic and soft optic modes, and solid lines correspond to coupled modes.

$$\ddot{Q}_k+\omega_0^2 Q_k+i\alpha\mathbf{k}Z_k=0, \tag{10}$$

$$\ddot{Z}_k+\omega_{\mathrm{TA}}^2 Z_k-i\alpha\mathbf{k}Q_k=0, \tag{11}$$

which for trial solutions $\ddot{Q}_k=-\Omega^2 Q_k$ and $\ddot{Z}_k=-\Omega^2 Z_k$ reduce to

$$(\omega_0^2-\Omega^2)Q_k+i\alpha\mathbf{k}Z_k=0, \tag{12}$$

$$(\omega_{\mathrm{TA}}^2-\Omega^2)Z_k-i\alpha\mathbf{k}Q_k=0. \tag{13}$$

The corresponding secular equation takes a simple form:

$$\begin{vmatrix} \omega_0^2-\Omega^2 & i\alpha\mathbf{k} \\ -i\alpha\mathbf{k} & \omega_{\mathrm{TA}}^2-\Omega^2 \end{vmatrix}=0 \tag{14}$$

and has two analytical solutions:

$$\Omega_{\pm}^2=\frac{1}{2}\{(\omega_0^2+\omega_{\mathrm{TA}}^2)\pm[(\omega_0^2-\omega_{\mathrm{TA}}^2)^2+4\alpha^2\mathbf{k}^2]^{1/2}\}. \tag{15}$$

These results are summarized in Fig. 9 where the dispersion curves of ''uncoupled'' and ''coupled'' modes are shown. The bilinear interaction between the optical and acoustical modes leads to the ''repulsion'' of the optical and acoustical branches resulting thus to the decrease in the slope of the lower acoustical branch $\Omega_-(\mathbf{k})$. The phase transition occurs at a certain $P=P_0$, where the slope of the acoustical branch $\Omega_-(q)$ equals zero at $\mathbf{k}\to 0$ {i.e., $d\Omega_-(\mathbf{k})/d\mathbf{k}|_{k\approx 0}\equiv[\Omega_-(\mathbf{k})/\mathbf{k}]^2=0$}. This gives

$$\omega_0^2\omega_{\mathrm{TA}}^2=\alpha^2\mathbf{k}^2. \tag{16}$$

By taking into account that in the limit $\mathbf{k}\to 0$, $\omega_0^2\approx A_0(P_C-P_0)$ at $P=P_0$, Eq. (16) transforms into

$$P_0=P_C-\alpha^2/C_{44}^0 A_0. \tag{17}$$

It follows from Eq. (17), that the ferroelastic instability occurs at $P_0<P_C$, where the soft optical mode frequency ω_0 is still positive and real, whereas the phase velocity of the transverse-acoustic phonons $V_4=\sqrt{C_{44}/\rho}\sim\Omega_-(\mathbf{k})/\mathbf{k}$ tends to zero. This agrees with the results of calculations within the rigid-ion model, as well as with the experimental data presented in Fig. 1. The same result can be obtained directly from Eq. (5) for $\mathbf{k}=0$. After eliminating deformation U_4 from the free energy, we obtain

$$F=\frac{1}{2}A_0(P_C-P-\alpha^2/A_0C_{44}^0)Q^2, \tag{18}$$

which leads to the relation in Eq. (17). The phase velocity V_4 can easily be found using the Slonchewski-Thomas equation

$$C_{44}=C_{44}^0-\frac{\partial^2 F}{\partial Q\,\partial U_4}\left(\frac{\partial^2 F}{\partial^2 Q}\right)^{-1}\frac{\partial^2 F}{\partial Q\,\partial U_4}. \tag{19}$$

Inserting Eq. (5) into Eq. (19) one obtains

$$V_4=\frac{1}{\sqrt{\rho}}\left[C_{44}^0-\frac{\alpha^2}{A_0(P_0-P)+\alpha^2/C_{44}^0}\right]^{1/2}. \tag{20}$$

This equation clearly shows that $V_4\to 0$ for $P\to P_0$.

VII. CONCLUSIONS

We have here presented the lattice-dynamics analysis of Cs_2HgCl_4 crystals in the case where the pressure induces a proper ferroelastic instability. We have used a semiempirical rigid-ion model in the quasiharmonic approximation. The model parameters, i.e., the effective radii and charges, have been adjusted at $T=293$ K in order to satisfy the experimentally observed equilibrium configuration of the lattice structure. The calculated frequencies of the external phonon modes at $\mathbf{k}=0$ are in good agreement with Raman scattering data. The influence of unharmonicity, which is a general reason for the lattice instability at second-order phase transitions, has been indirectly introduced into the lattice-dynamics simulation through the changes of the lattice parameters that occur under the action of hydrostatic pressure and temperature. The changes of lattice parameters were estimated using the data of ultrasonic and dilatometric measurements. Such a simple model is already sufficient to reproduce quantitatively the phonon dynamics near the proper ferroelastic phase transition. Particularly, the present analysis supports the idea that the origin of the ferroelastic instability observed in these crystals is essentially related to the soft optical mode (B_{3g} symmetry at $\mathbf{k}=0$) and the transverse-acoustical mode $\mathrm{TA}_Z(\mathbf{k}\|\mathbf{b}^*)$. It is clearly shown that the lattice loses its stability with respect to the acoustical vibration whereas the soft optical mode remains stable at the phase-transition point. This conclusion is in excellent agreement with the predictions of the phenomenological theory and experimental data.

[1] S. A. Linde, A. Ya. Michailova, V. I. Pahomov, V. V. Kirilenko, and V. G. Shulga, Koord. Khim. **9**, 998 (1983) (Russian).
[2] S. N. Kallaev, V. V. Gladkii, V. A. Kirikov, and I. K. Kalimov, Ferroelectrics **106**, 229 (1990).
[3] A. A. Boguslavsky, R. Sh. Lotfullyn, and M. V. Smirnov, Fiz. Tverd. Tela (Leningrad) **27**, 523 (1983).
[4] A. V. Kityk, O. M. Mokry, V. P. Soprunyuk, and O. G. Vlokh, J. Phys.: Condens. Matter **5**, 5189 (1993).
[5] O. G. Vlokh, E. P. Kaminskaya, A. V. Kityk, A. P. Levanyuk, and O. M. Mokry, Sov. Phys. Solid State **31**, 1629 (1989).
[6] R. Blinc and B. Zeks, *Soft Modes in Ferroelectrics and Antiferroelectrics* (Elseiver, New York, 1974).
[7] E. P. Papadakis, J. Acoust. Soc. Am. **42**, 1045 (1967).
[8] O. G. Vlokh, V. G. Gribik, A. V. Kityk, O. M. Mokry, I. D. Olekseyuk, and S. A. Piroga, Kristallografiya **35**, 1483 (1990).
[9] A. V. Kityk, A. V. Zadorozhna, Ya. I. Shchur, I. Yu. Martynyuk-Lototska, and O. G. Vlokh (unpublished).
[10] S. L. Chaplot (unpublished).